Bulletin of Earthquake Engineering (2023) 21:2141–2171
https://doi.org/10.1007/s10518-022-01602-w

ORIGINAL ARTICLE

Identifying and modeling ductile RC columns with deformed bars

Mariano Di Domenico[1] · **Paolo Ricci**[1] · **Gerardo M. Verderame**[1]

Received: 22 July 2022 / Accepted: 13 December 2022 / Published online: 26 December 2022

Abstract

In this paper, empirical equations are proposed to calculate the moment-chord rotation response envelope of ductile rectangular reinforced concrete columns with deformed bars. The proposed envelope accounts for cyclic strength degradation and is defined by four characteristic points: yielding, maximum, conventional ultimate, and collapse. Also, the proposed envelope is implemented by adopting Pinching4 Material model in OpenSees and, based on the experimental data, the hysteretic parameters governing unloading and reloading stiffness degradation, as well as pinching effect, are calibrated. The proposed model is applied at the element level, thus showing the potential advantages and limitations of its use, also in comparison with other analogous proposals presented in the literature. The proposed model has two main advantages with respect to proposals existing in the literature: (i) the response envelope already includes cyclic degradation of force capacity, thus fulfilling the requests of current standards regarding the need of accounting for members' mechanical softening within nonlinear static procedures; (ii) the hysteretic parameters governing unloading and reloading stiffness degradation, and pinching, allow a more accurate reproduction of members' and structures' seismic response within nonlinear dynamic procedures.

Keywords Empirical · Model · Response · Hysteretic · Seismic · RC column

List of symbols

A_{sl}	Total area of longitudinal reinforcement
A_{sw}	Area of transverse reinforcement
d	Section effective depth
EI_y	Secant-to-yielding section stiffness
EI_g	Gross section stiffness

✉ Mariano Di Domenico
mariano.didomenico@unina.it

Paolo Ricci
paolo.ricci@unina.it

Gerardo M. Verderame
verderam@unina.it

[1] Department of Structures for Engineering and Architecture, University of Naples Federico II, Via Claudio 21, 80125 Naples, Italy

f_c	Concrete compressive strength
f_{yl}	Longitudinal steel yielding stress
f_{yw}	Transverse steel yielding stress
h	Section depth
L_s	Shear span
s	Transverse reinforcement spacing
ν	Axial load ratio
ρ_l	Geometrical longitudinal reinforcement ratio
ρ_w	Geometrical transverse reinforcement ratio
ω_1	Mechanical longitudinal reinforcement ratio in tension (including web reinforcement)
ω_2	Mechanical longitudinal reinforcement ratio in compression
ω_l	Mechanical longitudinal reinforcement ratio
ω_w	Mechanical transverse reinforcement ratio

1 Introduction

Nowadays, practitioners can design a new Reinforced Concrete (RC) Moment Resisting Frame (MRF) against seismic loads by adopting linear elastic analysis. In addition, they can perform the seismic assessment of an existing RC MRF building by adopting linear elastic analysis. However, it is well known that only nonlinear analysis can depict an accurate description of a RC MRF building performance, especially under cyclic seismic loads. This applies, above all, for the seismic assessment of existing buildings and applies for both practitioners and researchers. Namely, researchers interested in performing an extensive analysis of the seismic performance, up to real collapse, of a RC building cannot adopt other than nonlinear static or dynamic analysis.

For these reasons and for these aims, both practitioners and researchers need reliable models reproducing the cyclic force–displacement response of a structure as a whole; to do this, reliable models reproducing the cyclic force–displacement response of structural members are needed, in tune.

Nonlinear modeling of RC structural members can be performed by adopting a "Fiber" approach and a "Hinge" approach. In the first case, a certain number of the member cross-sections is discretized in fibers to which a certain stress–strain relation is assigned, based on the material of each fiber (namely, concrete and steel for RC cross-sections). Local and global equilibrium and compatibility conditions are enforced to derive, step-by-step during the nonlinear analysis, the cross-section force–deformation state and, consequently, the member force–deformation state and, consequently, the structure force–deformation state. On the other hand, "Hinge" approaches consist in assigning pre-determined empirical-based force–displacement response rules to structural members. These "rules" are "lumped" in a concentrated hinge placed at each end of a member. Local and global equilibrium and compatibility conditions are enforced to derive, step-by-step during the nonlinear analysis, the member force–deformation state and, consequently, the structure force–deformation state. Advantages and shortcomings of "Fiber" and "Hinge" approaches have been deeply discussed in the literature (see, for example, Spacone et al. 1996; Coleman and Spacone 2001; Rodrigues et al. 2012; Belletti et al. 2013; Vafei et al. 2019;

Terrenzi et al. 2020; Lima et al. 2020; Lee et al. 2021; Bruschi et al. 2021) and are not the core topic of this paper, which focuses on "Hinge" approaches.

More specifically, when modelling RC members with a "Hinge" approach, a plastic hinge is assigned to both ends of the member, each of which is governed by a pre-determined bending Moment (M)–chord rotation (θ) response. Such a kind of "macro-modeling" approach is based on a M–θ response whose characteristic points are calculated with the aim of reproducing the expected "real" response of each member, i.e., the response that it would exhibit during a cyclic experimental test. Generally, this response is characterized by an initial elastic or pseudo-elastic branch, by a hardening branch and by "softening" branch(es), as schematically shown in Fig. 1.

As shown in Fig. 1, the typical cyclic response of a real RC member can be schematized by defining four characteristic points: the yielding point, the capping/peak load point, the (conventional) ultimate point and the collapse point. While mechanical methods can be successfully adopted to predict moments at yielding and capping (the moment at ultimate is typically conventionally assumed equal to 80% of the capping moment, while the moment at collapse is equal to a residual value, potentially equal to zero for "real" collapse), chord rotation values corresponding to the characteristic points are usually determined by adopting empirical equations accounting for the presence of different sources of deformability, e.g. flexure, shear, and fixed-end rotation. It should be noted that this kind of response is actually exhibited by RC members if their failure is governed by flexure, i.e., if they are ductile; if their failure is governed by shear, they are classified as brittle and may show a steep softening after or even before yielding.

Focusing only on "complete" moment–chord rotation models, i.e., those including a softening branch up to zero lateral load capacity, recently, a response model was proposed by Di Domenico et al. (2021) for ductile RC columns with plain (also known as "smooth")

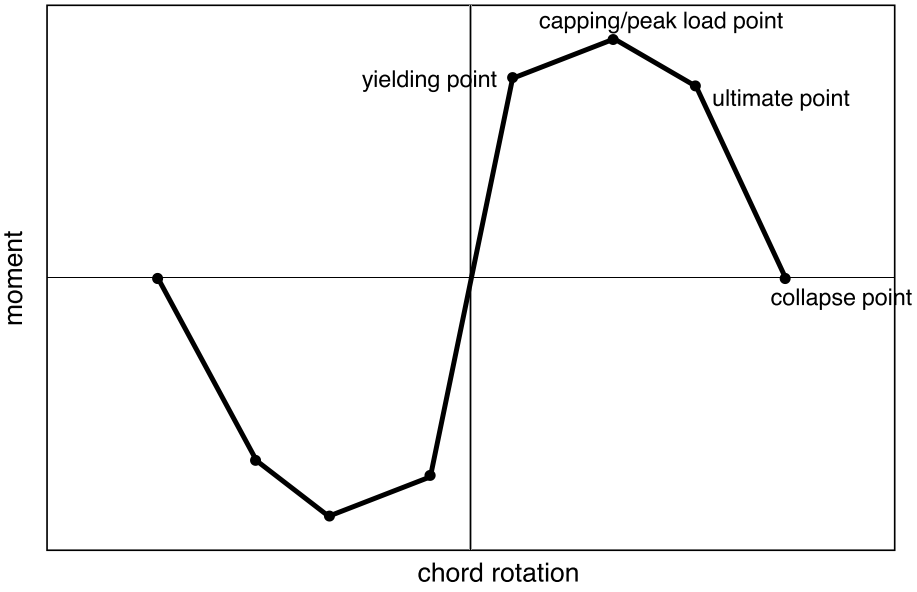

Fig. 1 Schematic moment-chord rotation response of a plastic hinge reproducing the lateral response of a RC column

bars; previously, a moment-chord rotation response rule was proposed by Haselton et al. (2008) for ductile RC columns with deformed (also known as "ribbed") bars.

In this paper, a moment-chord rotation empirical rule for modelling the lateral response of ductile RC columns with deformed bars under cyclic (such as seismic) load is proposed as an alternative to Haselton et al. (2008)'s approach. Note that equations for the assessment of the response envelope are proposed, as well as empirical parameters for reproducing unloading and reloading stiffness degradation due to cyclic loading and pinching effect. Section 2 presents the motivation for which the Authors are proposing an alternative to the existing and well-established proposal by Haselton et al. (2008). Section 3 describes the experimental database adopted for proposing an empirical-based method for identifying ductile RC columns (i.e., the kind of members for which the proposed model can be applied) (Sect. 4) and the equations for the prediction of the proposed moment-chord rotation response and the associated hysteretic parameters (Sect. 5). In Sect. 6, applications are presented to check the effectiveness of the proposed response model. Some conclusions are drawn in Sect. 7.

2 Motivation

As already mentioned, a complete moment–chord rotation law for reproducing the lateral response of ductile RC columns with deformed rebars already exists. It was proposed by Haselton et al. (2008), based on the experimental response of columns collected in the PEER Database (Berry et al. 2004). According to this model, which will be referred to as "Haselton et al. model" from here, a response envelope defined by three characteristic points (yielding, capping, ultimate) is defined, as shown in Fig. 2. Chord rotation values corresponding to these points are calculated by means of empirical equations including as predictor parameters some basic quantities referred to the

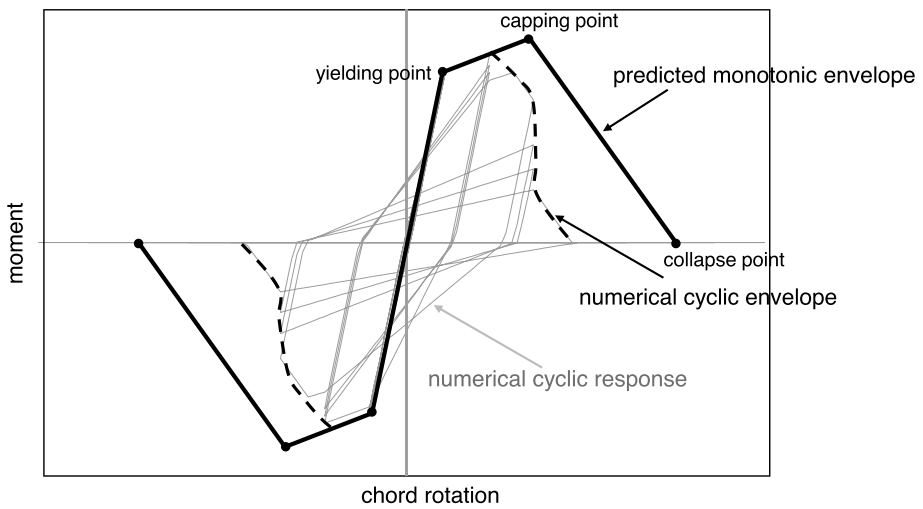

Fig. 2 Example of the monotonic response of a RC column predicted according to Haselton model (continuous black line) and of the cyclic response (continuous grey line) of the same column. The envelope of the cyclic response is represented by the dashed black line

column geometric and mechanical properties. Note that this envelope is referred to the monotonic response of the considered column. The model by Haselton et al. (2008) was implemented in the OpenSees software (McKenna et al. 2004) by using Modified Ibarra-Medina-Krawinkler (ModIMK) Peak-Oriented Material model and by activating the possibility of force degradation due to cyclic loading whose amount and evolution is governed by a "rate" parameter, λ. The rate parameter depends on the column axial load ratio, on the spacing of stirrups, and on the cross-section depth, based on the collected experimental data. In other words, as shown in Fig. 2, if a column is modelled by adopting Haselton model and is monotonically pushed, it will exhibit a certain moment (at the base of the column)–chord rotation response envelope; if it is cyclically pushed-pulled, it will exhibit a cyclic response, whose envelope is different from the monotonic envelope since force degradation is activated (only) during cyclic loading. Of course, if the members of an entire structure are modelled with this approach, also the structure will exhibit a different response envelope under monotonic lateral pushing (i.e., during monotonic pushover analysis) or under cyclic lateral loads (i.e., during time-history dynamic analysis).

Force degradation due to cyclic loading is a real phenomenon and must be considered when reproducing the nonlinear response of RC members and structures. As shown in Fig. 2, it significantly influences the lateral response of a member after yielding, by reducing capping moment and by anticipating and making steeper the softening branch which can be observed also under monotonic loading. In other words, adopting a response model calibrated on monotonic envelopes, such as Haselton et al. model, for performing a nonlinear static analysis may yield to a non-reliable assessment of the post-yielding and of the degrading response of the structure. This issue could be fixed by performing a cyclic pushover analysis, which is not widely adopted. Clearly, a reliable assessment of the post-yielding and post-peak response of a structure is fundamental for researchers adopting nonlinear static analysis. However, note that the American Standard ASCE-SEI 41/17 (ASCE 2017), in section 7.4.3.2 "Modeling and analysis considerations for NSP (Nonlinear Static Procedures)" states: "*the force–displacement behavior of all components shall be explicitly included in the model using full backbone curves that include strength degradation and residual strength, if any.*" In section 7.4.4.2, this statement is extended also for modeling aimed at performing nonlinear dynamic analyses. This means that to completely fulfil the ASCE Standard requirements for performing a reliable NSP analysis, there is need of a model accounting for force degradation in the most reliable way also under (equivalent) monotonic loading, such as in nonlinear static analysis.

Regarding nonlinear dynamic analyses, there are further issues not completely covered by Haselton et al. (2008) proposal: the seismic assessment of a structure could be influenced also by other cyclic degradation phenomena, namely unloading and reloading stiffness degradation and pinching effect. These effects can be considered also when adopting Haselton et al. model, but the hysteretic parameters governing them are not explicitly calibrated.

In this paper, based on ACI 369 rectangular column database (Sivaramakrishnan 2010), which is wider than PEER database, equations for the assessment of the response envelope of ductile RC columns are proposed. Since only columns tested under cyclic loading are considered (see Sect. 3 for more details), the resulting proposed response envelope already contains the effect of force degradation due to cyclic loading, thus yielding to the possibility of performing a NSP completely fulfilling ASCE Standard requirements without need of more complex cyclic pushover analysis. Also, the proposed equations are set together with the calibration of parameters aimed at reproducing also the effects of pinching and

unloading and reloading stiffness degradation under cyclic loads on the lateral response of members. This may allow a more accurate assessment of a RC moment-resisting frame seismic performance via nonlinear dynamic analysis, a seismic analysis method more and more diffused among both practitioner and researchers.

Differently from Haselton et al. model, which is implemented in OpenSees software by adopting ModIMKPeakOriented Material rules, the response model proposed in this paper is conceived to be implemented by adopting Pinching4 Material (which has been similarly adopted to model the cyclic response of RC columns with plain rebars by the Authors of this study). This material model allows the definition of a 4-point response envelope together with cyclic degradation parameters for modelling pinching, unloading and reloading stiffness, and strength degradation. More details on this topic are provided in Sect. 5. However, note that the proposed response envelope, already including cyclic strength degradation, can be adopted for modeling the lateral response of RC members with whichever software that allows the user defining the response envelope of structural members.

However, before presenting the model equations and cyclic parameters, it is necessary to present the experimental database based on which these empirical equations and parameters have been determined, as well as to answer to a fundamental question: given a certain RC column, how to establish if the proposed model is applicable, i.e., how to establish if the considered column is ductile?

3 Reference experimental database

The proposed model is based on the experimental data collected in the ACI 369 Rectangular Column Database (Sivaramakrishnan 2010), which will be briefly named "ACI database" in the following.

The ACI database is constituted by 326 cyclic tests performed on rectangular RC columns. In this work, only cyclic tests of rectangular columns are considered. All specimens are characterized by the presence of deformed longitudinal rebars, while transverse reinforcement may be realized with deformed or plain bars. For each specimen, the following data are reported:

- Material properties (for concrete, longitudinal and transverse reinforcement);
- Column geometry (for the overall column, longitudinal and transverse reinforcement);
- Confinement details (i.e., the configuration of transverse reinforcement);
- Test configuration details (i.e., how the lateral load was applied on the specimen);
- Test results in terms of observed failure mode, significant values of force and displacement, force–displacement loops (if available).

Note that no information is provided about the presence or absence of seismic detailing in the specimens. This is a deliberate choice, due to the difficulty of determining a unique definition of "seismic detailing" applicable to columns tested in different ages and in different parts of the world.

As already mentioned, the correct identification of ductile columns is a core issue of this work since it establishes the basic applicability condition of the proposed empirical model. So, it is worth mentioning how the definition of the failure mode was performed by the Authors of ACI database. Two approaches are considered for failure mode classification: the first one is consistent with the approach adopted by PEER in Berry et al.

(2004) and is more based on the "observed" response of the specimens; the second, which is more "practice-oriented", is based on the assessment of transverse reinforcement detailing and on the ratio between the plastic shear demand and the expected shear capacity. The discussion presented in this paper is based on the first classification approach, i.e., the one consistent with PEER, since it is independent on the assessment of shear strength by means of a specific shear capacity model. In fact, consistently with the PEER approach, a first distinction is made between shear-sensitive and non-shear-sensitive members. If the Authors of each experimental test report the occurrence of shear damage for a certain specimen, the element is classified as "shear critical". Otherwise, it is classified as "flexure critical", i.e., ductile, and the assigned failure mode is identified as "F".

Among shear critical elements, a mixed analytical/empirical approach is adopted to distinguish elements between those exhibiting a shear failure before or after yielding (identified as "S" or "FS" elements, respectively). First, for each specimen, the maximum lateral force attained (F_{eff}) is evaluated. Then, the theoretical maximum force corresponding to the attainment of a maximum strain in concrete equal to 0.4% ($F_{0.004}$) is calculated. In addition, based on the experimental response of the specimen, the ductility capacity μ_{fail} is calculated by assuming as failure displacement the one associated with a force capacity equal to 0.80 times F_{eff} on the softening branch of the force–displacement response. If F_{eff} is lower than 0.95 times $F_{0.004}$ or μ_{fail} is equal or lower than 2, the shear critical element is classified as S. Otherwise, it is classified as FS.

Among the 326 tests collected in the database, only those for which all the significant geometric, mechanical and response parameters were available have been used for this study. In addition, only "completely cyclic" tests were considered: in other words, test with monotonic loading before and/or after yielding were excluded. In addition, columns with spliced reinforcement were excluded since they can undergo a premature failure due to insufficient anchorage length, as shown, for example, for the specimens by Melek and Wallace (2004) that are included in the original ACI dataset but are not considered for this study. Hence, a subset of the ACI database constituted by 225 tests is considered in this work. In this reference subset, hereinafter named "reference database", 156 tests are classified as F while 69 tests are classified as FS. As will be shown in the next sections, FS tests were considered only to derive experimental data related to the chord rotation at yielding.

As shown in Fig. 3, the tests collected in the reference database are characterized by $0 \le \nu$ (axial load ratio) ≤ 0.90, $13 \le f_c$ (compressive strength of concrete) ≤ 118 N/mm^2, $323 \le f_{yl}$ (yielding stress of longitudinal rebars) ≤ 587 N/mm^2, $255 \le f_{yw}$ (yielding stress of transverse rebars) ≤ 1424 N/mm^2, $0.0068 \le \rho_l$ (longitudinal reinforcement ratio) ≤ 0.0603, $0.0006 \le \rho_w$ (transverse reinforcement ratio) ≤ 0.0321, $1.27 \le L_s/d$ (shear span-to-effective depth aspect ratio of the element) ≤ 8.90, $0.11 \le s/d$ (transverse reinforcement spacing-to-effective depth of the cross section ratio) ≤ 1.27. These bounds define the applicability ranges of the proposed model. Note also that the considered tests were performed by adopting different cyclic loading protocols, namely by imposing to the specimen the same target top displacement once, twice, or three times (the most adopted one) before passing to the application of a higher target top displacement. However, despite this variety of loading protocols, it should be noted that the proposed cyclic model, differently from the monotonic response model by Haselton et al. (2008), is implicitly influenced by the loading protocols adopted for tests, as well as by their "conventional" nature.

Note also that ACI database includes 36 S tests. These have been considered only when defining straightforward criteria for the assessment of the expected failure mode of columns (see Sect. 4).

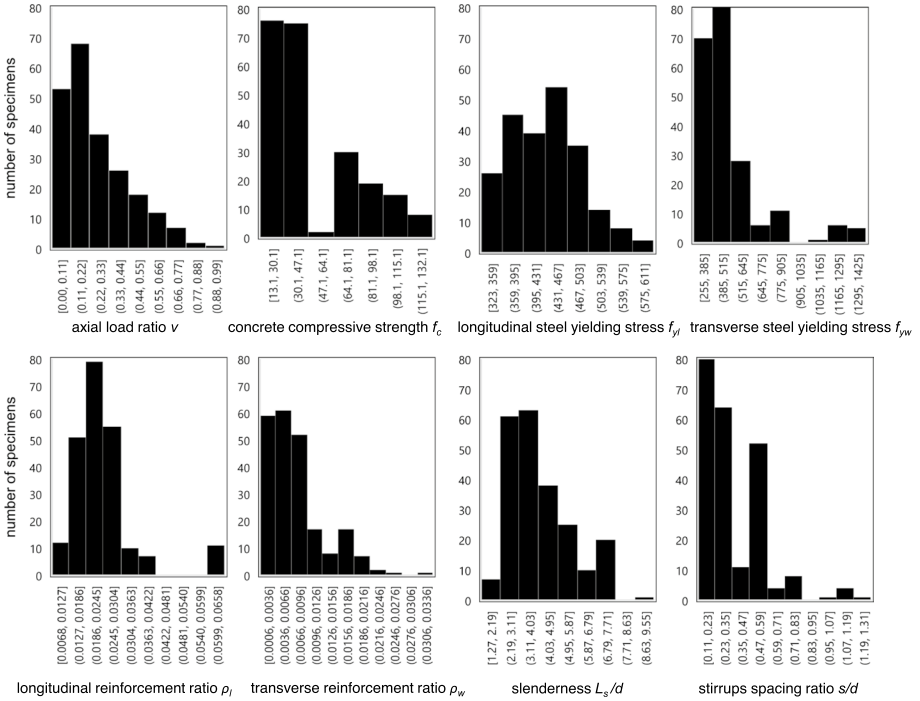

Fig. 3 Distribution of the geometric and mechanical properties of the specimens included in the selected database

Note that the experimental response loops of specimens were corrected, if necessary, to remove the spurious effect given by geometric non-linearity (i.e., P–Δ effects) and, so, consider only mechanical sources triggering the post-peak softening. The correction has been performed to lead back the experimental response of the selected specimens to "Case I" according to Berry et al. (2004).

ACI database is described more in details in Sivaramakrishnan (2010).

4 Identyifing ductile RC columns

In general, the distinction between shear critical and flexural critical columns can be performed via a "static" approach by comparing the shear demand at yielding V_y (i.e., the shear demand in equilibrium with the yielding moment acting at the fixed end(s) of the column) and the shear demand at maximum V_{max} (i.e., the one in equilibrium with the maximum moment acting at the fixed end(s) of the column), with the shear resistance of the column, V_R, whose value is maximum under monotonic load and decreases, up to a minimum, due to cyclic ductility demand (Priestley et al. 1994; Sezen and Moehle 2004; Biskinis et al. 2004). A member is flexure critical (i.e., it cannot undergo a brittle failure) if V_{max} is lower than the minimum possible value of V_R; otherwise, it is shear-critical, i.e., it may undergo a brittle failure. The application of this procedure for failure mode prediction needs the selection of a certain shear strength model and its results sensitively depend on

it. Here, an empirical and straightforward failure mode classification procedure, based on the ACI database, independent on a specific shear strength model, is proposed. It should be intended as a preliminary check for the applicability of the proposed response model: if a RC column has rectangular section and is ductile according to the proposed procedure, the proposed response model could be adopted.

To this aim, a set of potential predictive parameters was selected, based on previous literature studies (e.g., Ghannoum 2017; Ma and Gong 2018) and their expected mechanical influence; they are reported as follows: axial load ratio, ν; cross section height-to-shear span aspect ratio, h/L_s; longitudinal-to-transverse mechanical reinforcement ratio, ω_l/ω_w.

To analyze the effect of each potential predictor on the expected failure mode, for each potential predictor the collected database is divided in ten roughly equi-populated bins, with each bin constituted by 25 or 26 tests. In each bin, the frequency of observing an F, an FS or an S failure is calculated by dividing the number of specimens belonging to that bin and exhibiting an F, an FS or an S failure by the total number of specimens belonging to that bin.

The axial load ratio, ν, is calculated as the ratio between the axial load applied on the column during the test and the product of A_g, the gross area of the cross-section times f_c, concrete compressive strength. It should be considered that at increasing axial load ratio,

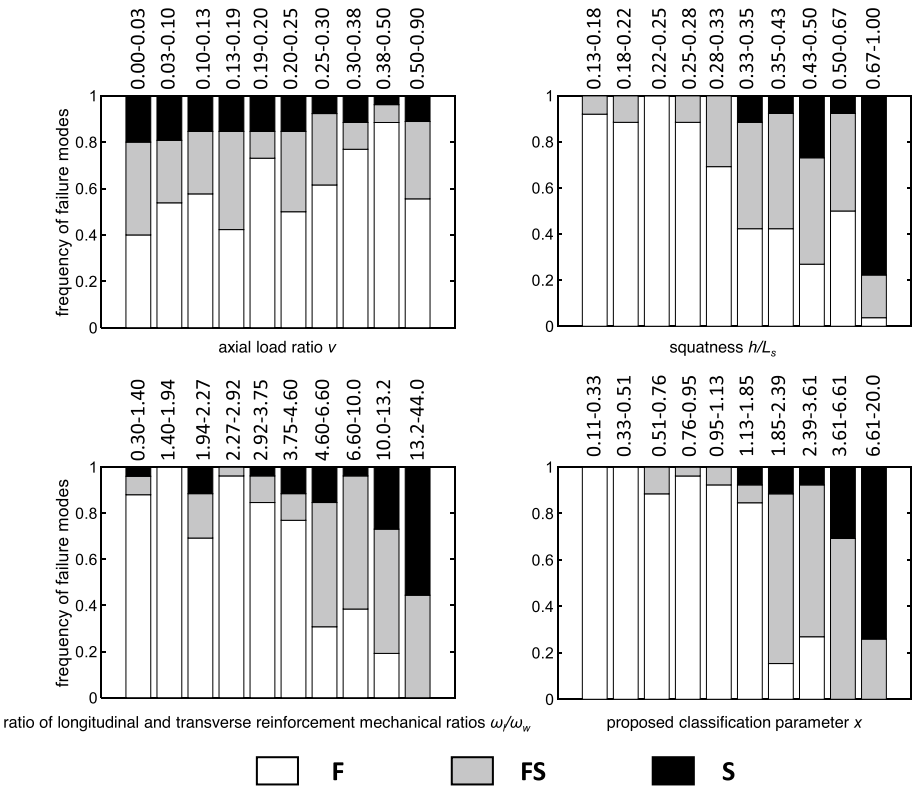

Fig. 4 Frequency of the observed failure mode for the RC columns of the selected database for varying geometric and mechanical properties of the columns

both the maximum moment (i.e., V_{max}) and the shear resistance V_R, increase up to a certain level of axial load ratio, and then decrease. So, a specific trend for the frequency of each failure mode at increasing ν is not expected. This is confirmed also by Fig. 4.

The aspect ratio is the ratio between the height of the cross section, h, and the shear span of the column, L_s. It is well known that slender elements (i.e., those with low h/L_s) tend to be flexure critical, while squat elements (i.e., those with high h/L_s) tend to be shear critical. This is confirmed also by Fig. 4.

The longitudinal-to-transverse mechanical reinforcement ratio, ω_l/ω_w, is calculated as given in Eq. 1, in which A_{sl} is the total area of longitudinal reinforcement in the cross section, A_{sw} is the total area of transverse reinforcement in the cross section, f_{yl} is the yielding stress of the longitudinal rebars, f_{yw} is the yielding stress of the transverse reinforcement, f_c is concrete compressive strength, d is the effective depth of the cross section, b is the width of the cross section, s is the spacing of transverse reinforcement.

$$\frac{\omega_l}{\omega_w} = \frac{A_{sl}f_{yl}}{dbf_c}\frac{sbf_c}{A_{sw}f_{yw}} = \frac{s}{d}\frac{A_{sl}f_{yl}}{A_{sw}f_{yw}} \tag{1}$$

Since ω_l is an index positively correlated with the member yielding moment/yielding shear while ω_w is an index positively correlated with the member shear strength, it is expected that the higher ω_l/ω_w, the higher the ratio between V_y and V_R. As already mentioned, if V_y is higher than V_R, the member is shear critical. So, at increasing ω_l/ω_w, an increasing frequency of FS and S failures is expected. This is confirmed also by Fig. 4.

For these reasons, it is expected that a combined dimensionless parameter given by the product of h/L_s times ω_l/ω_w may be a good predictor parameter. This is confirmed by the experimental database as shown in Fig. 4, in which clear (and expected) trends of the frequency of F, FS and S failure modes are observed at increasing h/L_s times ω_l/ω_w value, together with a "full reversal" from a "total flexure critical" first bin to a "total shear critical" last bin. For this reason, h/L_s times ω_l/ω_w is selected as predictive parameter and is named x, as given in Eq. 2.

It is observed that for x lower than 1, no S failure is detected and that most of the column is classified as F, with some FS cases. However, only columns with x lower than 0.70 are always classified as ductile. So, it is concluded that the proposed model can be applied only for x lower than 0.70. However, since FS tests' results are used for the proposal of the empirical equation for predicting the secant-to-yielding stiffness, only this equation can be adopted also for columns with x between 0.70 and 1.

$$x = \frac{h}{L_s}\frac{\omega_l}{\omega_w} = \frac{h}{L_s}\frac{s}{d}\frac{A_{sl}f_{yl}}{A_{sw}f_{yw}} \tag{2}$$

The proposed predictor parameter and its limit value for ductile columns may have a potential application also in the design process of RC members. In fact, it has been empirically observed that RC columns exhibit a ductile response if x is lower than or equal to 0.70. This condition, explicated in Eq. 3, may be used for a straightforward dimensioning of transverse reinforcement amount (namely, the spacing of transverse reinforcement in the critical regions of RC members) in order to ensure the fulfilment of capacity design rules at the element level.

$$x \le 0.70 \Rightarrow \frac{h}{L_s}\frac{s}{d}\frac{A_{sl}f_{yl}}{A_{sw}f_{yw}} \le 0.70 \Rightarrow s \le 0.70\frac{L_s}{h}\frac{A_{sw}}{A_{sl}}\frac{f_{yw}}{f_{yl}}d \quad (3)$$

Usually, longitudinal and transverse reinforcement have the same design yielding stress. Moreover, for design purposes, d is usually assumed equal to 0.90 times h. Based on this, Eq. 3 simplifies in Eq. 4. This simplification is conservative, since the yielding stress is typically higher for the steel of rebars with smaller diameter and, usually, transverse reinforcement is realized with rebars with smaller diameter with respect to those used for longitudinal reinforcement.

$$s \le 0.60\frac{A_{sw}}{A_{sl}}L_s \quad (4)$$

5 Modeling ductile RC columns

Based on the envelope of the experimental response of ductile members included in the database, the following characteristic points/conditions were defined:

- The first point of the proposed envelope is first yielding point. First, a theoretical prediction of M_y was obtained by means of a fiber section analysis and indicated as $M_{y,fiber}$. Fiber section analyses were performed by assigning an elastic–plastic response to longitudinal steel rebars, with elastic modulus E_s equal to 210,000 N/mm^2 and strain at yielding $\varepsilon_{sy}=f_{yl}/E_s$, and the response envelope defined by Mander et al. (1988) for unconfined concrete to concrete, with elastic modulus equal to $5000\sqrt{f_c}$ and strain at peak stress ε_{c0} equal to 0.002. $M_{y,fiber}$ is the moment for which the strain of the outermost compressed concrete fiber attains ε_{c0} or the maximum (in absolute value) strain of the longitudinal reinforcement layer more distant from the neutral axis and in tension attains ε_{sy}, whichever occurs first. Note that the first yielding point is defined similarly by Priestley et al. (2007), that also provided a definition of "nominal" yielding which was not used for this study (i.e., experimental response envelopes were not "bilinearized"). Then, the experimental maximum moment M_{max} was determined. If M_{max} resulted higher than $1.07M_{y,fiber}$, the yielding point was identified on the experimental envelope at the attainment of base moment equal to $M_{y,fiber}$; otherwise (a condition more frequent for FS tests), according to Elwood and Eberhard (2009), the yielding point was identified on the experimental envelope at the attainment of base moment equal to $0.80M_{max}$. For the determination of first yielding point, all F and FS tests of the database were considered, for a total of 225 data.
- The second point of the envelope is the peak load or capping point. It was simply determined at the attainment of a moment equal to the maximum moment M_{max}. For the determination of this point, 112 out of 156 F tests of the database were considered, i.e., only those F tests for which the attainment of capping point was clear (i.e., those showing a descending branch up to 5% of strength degradation).
- The third point of the envelope was determined on the descending branch of the experimental response envelope at the attainment of a moment equal to $0.80M_{max}$. This point

corresponds to the attainment of a conventional ultimate condition. For the determination of this point, 49 F tests were considered.

- The fourth and last point of the envelope is the one corresponding to the complete loss of lateral load capacity of the column. It was determined, on the experimental envelope, by linear extrapolation up to zero moment resistance of the extreme points of the imposed displacement cycles defining the descending branch of the experimental envelope beginning from the experimental point at conventional "ultimate", as defined at the previous point. Note that, to limit the use of unreliable extrapolated data, only tests for which at least a 50% strength decrease after peak load point attainment were considered for the assessment of this point. For the determination of this point, 15 F tests were considered.

A consistent approach was adopted to define an equivalent set of predictive equations for the assessment of the response envelope of rectangular RC column with plain bars in Di Domenico et al. (2021).

The following response parameters were adopted to identify the abovementioned characteristic points of the response envelope, as shown in Fig. 5.

- The ratio between the flexural secant stiffness at yielding of the member cross-section EI_y, and the flexural stiffness of the gross section EI_g. This ratio allows defining, together with the yielding moment M_y previously defined, the chord rotation at yielding, θ_y;
- The maximum moment M_{max} together with the corresponding post-yielding plastic chord rotation, θ_{max}^{pl};
- The post-capping plastic chord rotation at conventional "ultimate" condition, θ_{ult}^{pc};
- The post-ultimate plastic chord rotation at the attainment of zero lateral load capacity, θ_0^{pu}.

In order to define empirical formulations for the prediction of the abovementioned response parameters, some potential predictors were selected. The candidate predictors were chosen by considering the outcomes of past studies (e.g., Haselton et al. 2008), as well as their expected mechanical influence. In addition to those listed for the description

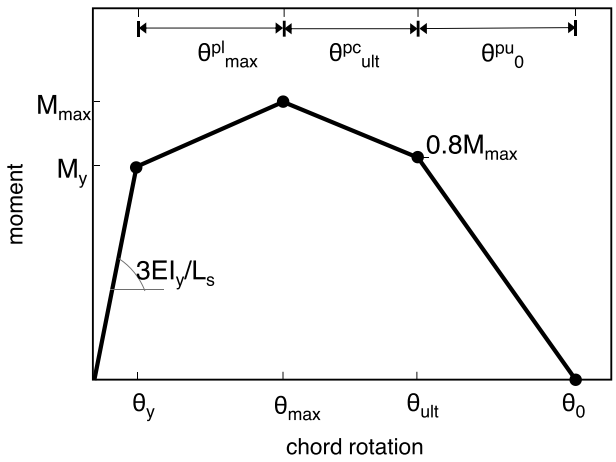

Fig. 5 Proposed envelope of the cyclic response of a RC column with deformed bars

of the experimental database (see Sects. 3 and 4), some combinations of them were assumed as potential predictive parameters, namely:

- The ratio between the spacing of transverse reinforcement, s, and the cross-section depth, d;
- The ratio between the spacing of transverse reinforcement, s, and the diameter of longitudinal rebars, d_b;
- The area/mechanical ratio of longitudinal rebars ρ_l and ω_l;
- The area/mechanical ratio of transverse reinforcement ρ_w and ω_w;
- The longitudinal reinforcement area/mechanical ratio calculated by separating the contribution of reinforcement in compression (ρ_2 and ω_2, respectively) from the contribution of reinforcement in tension + web reinforcement (ρ_1 and ω_1, respectively);
- The ratio between the area/mechanical longitudinal reinforcement ratio for rebars in compression and the mechanical longitudinal reinforcement ratio for rebars in tension.

The statistical procedure adopted for defining the predictive equations below listed is described in detail in Verderame and Ricci (2018). More specifically, linear least squares regressions were performed relating the output variables (expressed in terms of natural logarithm) and the potential predictors (expressed in their natural form, in terms of natural logarithm, or absent). The final equations proposed were selected among the ones with the minimum number of input variables but deemed as "statistically equivalent"—based on F-tests—to the basic predictive equations including all the potential predictors. For the assessment of predictive equations, T-tests were performed to remove outliers from the experimental database (Rosner 1983).

5.1 Predictive equations for the response envelope

The equations derived to define the response envelope of ductile rectangular RC columns with deformed bars are reported below, together with, for each proposed equation, the statistics—mean, median and Coefficient of Variation (CoV)—associated with the set of the observed value-to-predicted value ratios for the entire experimental database. In the proposed equations, forces must be expressed in Newtons and lengths in millimetres. Further details about the proposed equations and their capability of reproducing experimental outcomes are reported in the Appendix to this paper.

The ratio between secant-to-yielding and gross section stiffness, EI_y/EI_g can be calculated as reported in Eq. 5 (observed-to-predicted ratio: mean = 1.09, median = 1.00, CoV = 0.42). The corresponding initial stiffness of the response envelope of the member is $K_y = 3EI_y/L_s$.

$$EI_y/EI_g = 0.0318 \cdot 6.11^{\nu} \cdot \left(L_s/d\right)^{1.21} \simeq 0.0318 \cdot 6.11^{\nu} \cdot (1.639\left(L_s/d\right) - 1.110) \quad (5)$$

Alternatively, the ratio between secant-to-40% of yielding moment and gross section stiffness, EI_{40}/EI_g can be calculated as reported in Eq. 6 (observed-to-predicted ratio: mean = 1.13, median = 0.99, CoV = 0.49). The corresponding initial stiffness of the response envelope of the member is $K_{40} = 3EI_{40}/L_s$.

$$EI_{40}/EI_g = 0.100 \cdot 3.20^{\nu} \cdot \left(L_s/d\right)^{0.871} \quad (6)$$

Note that both Eqs. 5 and 6 were obtained by considering not only F, but also FS specimens included in the database.

The post-yielding plastic chord rotation, θ_{max}^{pl} can be calculated as reported in Eq. 7 (observed-to-predicted ratio: mean = 1.15, median = 0.97, CoV = 0.54).

$$\theta_{max}^{pl} = 0.0073 \cdot 0.436^{\nu} \cdot (s/d)^{-0.261} \cdot 1.05^{100\omega_2} \tag{7}$$

For the calculation of the peak resistance, a simple mean value is proposed attempting to predict the M_{max}/M_y ratio, i.e., $M_{max}/M_y = 1.31$ (observed-to-predicted ratio: CoV = 0.15), with M_y calculated by means of a section fiber analysis.

The post-capping "ultimate" plastic chord rotation, θ_{ult}^{pc} can be calculated as reported in Eq. 8 (observed-to-predicted ratio: mean = 1.16, median = 0.99, CoV = 0.58).

$$\theta_{ult}^{pc} = 0.0126 \cdot 0.161^{\nu} \cdot 5.66^{\omega_l} \cdot 1.88^{100\rho_w} \tag{8}$$

The post-ultimate plastic chord rotation towards zero resistance, θ_0^{pu} can be calculated as reported in Eq. 9 (observed-to-predicted ratio: mean = 1.15, median = 1.02, CoV = 0.55). It is limited to the maximum value of θ_0^{pu} observed in the database.

$$\theta_0^{pu} = min\left(0.065; 0.0146 \cdot 0.021^{\nu} \cdot (100\omega_w)^{0.918}\right) \tag{9}$$

To avoid modelling issues, namely, to avoid that the bilinear softening branch of the response envelope is characterized by decreasing (in absolute value) softening stiffness, the post-ultimate plastic chord rotation resulting from Eq. 9 must be further limited according to Eq. 10.

$$\theta_0^{pu} \leq 4\theta_{ult}^{pc} \tag{10}$$

5.2 Hysteretic parameters

Once the four-point cyclic response envelope has been defined by means of the previous formulations, hysteretic parameters, based on experimental data, are calibrated in order to reproduce the most significant cyclic degradation phenomena, such as the degradation of unloading and reloading stiffness and the pinching effect.

Pinching4 Uniaxial Material model in OpenSees (McKenna et al. 2004) allows reproducing all these phenomena. A detailed description of Pinching4 Uniaxial Material

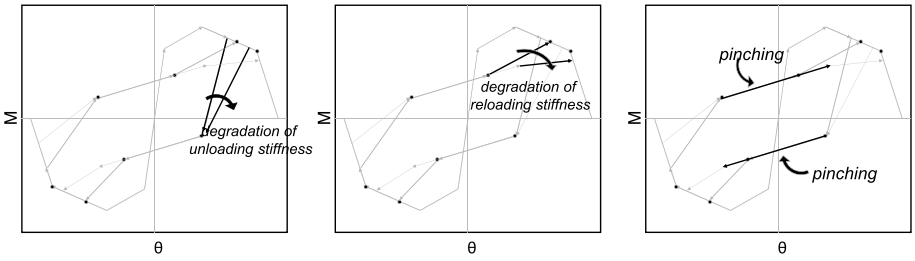

Fig. 6 Cyclic degradation phenomena considered in this study and modeled according to Pinching4 Uniaxial Material model in OpenSees

model is reported in (Lowes et al. 2004). In summary, it is worth mentioning that the degradation of unloading stiffness and reloading stiffness, as shown in Fig. 6, is modelled as a function of the displacement/chord rotation demand and of the energy dissipation terms combined by means of five parameters (for each degradation phenomenon) which have been experimentally calibrated. For example, the unloading stiffness at the i-th loading step, K_i, is calculated as reported in Eq. 11.

$$K_i = K_0\left(1-\delta k_i\right) = K_0\left(1-\left(gK1\theta_i^{*gK3}+gK2E_i^{*gK4}\right)\right) \le K_0(1-gKLim) \quad (11)$$

In Eq. 11, K_0 is the initial stiffness of the response envelope, θ_i^* is the chord rotation demand at the i-th loading step normalized with respect to the collapse one, θ_0, E_i^* is the dissipated energy up to the i-th loading step normalized with respect to the energy associated with the complete monotonic response envelope, $gK1$, $gK2$, $gK3$, $gK4$, and $gKLim$ are the abovementioned empirical parameters to be calibrated. A similar equation is adopted to model the degradation of reloading stiffness. The pinching effect is modelled by means of six (three for each loading direction) parameters which have been experimentally calibrated, too. The parameters to be calibrated are summarized in Table 1.

The calibration procedure is analogous to the one applied for determining the same hysteretic parameters for modelling the cyclic response of RC columns with plain bars (Di Domenico et al. 2021). It has been applied only on the 49 tests of the selected database allowing the calibration of the response envelope at least up to the attainment of ultimate chord rotation. This has been done to perform a parameter calibration not too much influenced by the cyclic response of columns in the pre-peak stage (remember that most of the columns of the selected database, unfortunately, are tested only up to the attainment of capping point) and, so, adequately representative of both the pre- and the post-peak stage of the response.

In summary, for each experimental test, the evolution of unloading and reloading stiffness has been evaluated (as shown in Fig. 6) as a function of the increasing imposed displacement demand and of the energy dissipation. After that, a nonlinear least-square regression analysis is performed, for each experimental test, to evaluate the values to be assigned to the parameters listed in Table 1 in order to have the better prediction of the actual degradation of unloading and reloading stiffness. For example, the parameters gKi to be included in Eq. 11 have been calibrated for each experimental test, separately, in order to have predicted Ki values consistent with the experimental ones.

Once these parameters have been calibrated, the parameters for pinching effect, which have been assumed equal for positive and negative loading direction, are calibrated by means of a trial-and-error procedure aimed at reproducing the evolution of

Table 1 List of the hysteretic parameters of Pinching4 Uniaxial Material model in OpenSees calibrated in this study

Cyclic degradation phenomenon	Parameters to be calibrated					
Unloading stiffness	gK1	gK2	gK3	gK4	gKLim	
Reloading stiffness	gD1	gD2	gD3	gD4	gDLim	
Pinching effect	rDisp (+)	rForce (+)	uForce (+)	rDisp (−)	rForce (−)	uForce (−)

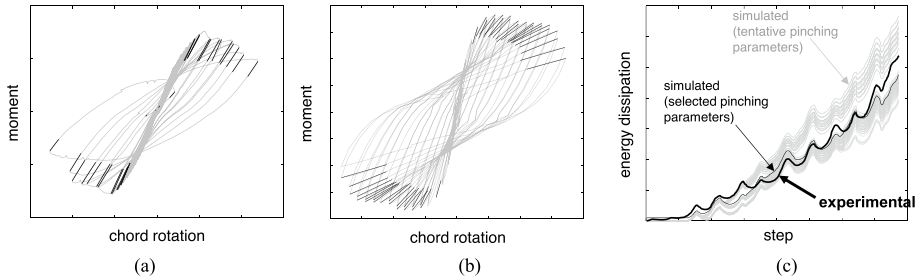

Fig. 7 Example of the assessment of unloading stiffness degradation for test ORC3 by Aboutaha and Machado (1999) (**a**), of reloading stiffness degradation for test C1-1 by Mo and Wang (2000) (**b**), and of pinching parameters, based on the simulation of dissipated energy, for test No. 7 by Watson and Park (1989) (**c**)

energy dissipation during the experimental tests with a numerical analysis performed by adopting the selected parameters, as shown in Fig. 7, in the more accurate way.

Note that the hysteretic parameters for modeling force degradation, an available feature of Pinching4 Material model, were not calibrated and must be set to zero, since the proposed empirical response envelope already includes the effect of cyclic force degradation (differently from the response envelope of Haselton et al. model).

After that, a total of 13 parameters have been calibrated for each test: in other words, 49 values for all the parameters have been determined. First, the Authors tried to find trends relating each parameter with geometric and mechanical features of the considered columns. Unfortunately, as already occurred for columns with plain bars (Di Domenico et al. 2021), no clear trend was found allowing the calculation of the hysteretic parameters as a function of geometric or mechanical features of a column. This should not surprise the reader, since hysteretic degradation is an overly complex phenomenon affected by strong aleatory uncertainty and experimental variability. The mean, median and standard deviation of the collected values are reported in Table 2. Note that *gKLim* value is assumed equal to 0.99 (this

Table 2 Statistics of the calibrated values of the hysteretic parameters

Parameter	gK1	gK2	gK3	gK4	gKLim
Mean	0.189	0.122	0.428	0.476	0.990
Median	0.074	0.053	0.460	0.412	(Assumed value)
Standard deviation	0.252	0.181	0.285	0.407	(Assumed value)

Parameter	gD1	gD2	gD3	gD4	gDLim
Mean	0.967	0.844	0.350	0.265	0.434
Median	0.153	0.363	0.237	0.053	0.500
Standard deviation	2.57	1.34	0.380	0.374	0.130

Parameter	rDisp	rForce	uForce
Mean	0.053	0.796	0.235
Median	0.110	0.860	0.370
Standard deviation	0.423	0.185	0.505

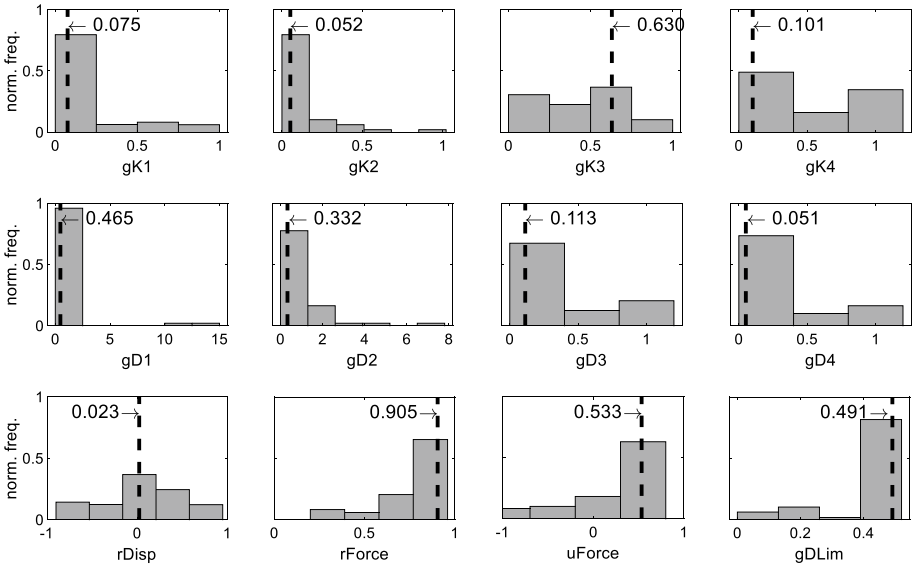

Fig. 8 Distribution of cyclic parameters determined for the selected subset of the database and selection of the proposed average values for modeling. "Norm. freq." is for "normalized frequency" and indicates, for each bin, the ratio between the number of tests with a calibrated parameter included in that bin divided by the total number of tests included in the selected subset of the database

Table 3 Values of the hysteretic parameters proposed for modeling

Parameter	gK1	gK2	gK3	gK4	gKLim
proposed value	0.075	0.052	0.630	0.101	0.990
Parameter	gD1	gD2	gD3	gD4	gDLim
proposed value	0.465	0.332	0.113	0.051	0.491
Parameter	gF1	gF2	gF3	gF4	gFLim
proposed value	0	0	0	0	0
Parameter	rDisp (+)	rForce (+)	uForce (+)	rDisp (−)	rForce (−)	uForce (−)
proposed value	0.023	0.905	0.533	0.023	0.905	0.533

means that the unloading stiffness can decrease from the initial one to 0.01 times the initial one, a limit imposed to avoid convergence issue or negative unloading stiffness).

It is proposed to adopt average values for the above-described parameters when modelling, independently on the column geometric and mechanical features. However, to avoid using average values affected by potential extreme data, the following procedure was adopted for each hysteretic parameter. First, the 49 calibrated values are divided into subsets (also named "bins") whose "width" is determined by means of Scott's formula (Scott 1979). As shown in Fig. 8, this allows determining, for each parameter, the bin containing the higher amount of data points normalized with respect to the available amount of data

(equal to 49, as already mentioned). The proposed average value is calculated only with reference to the bin with the highest number of included data. In this way, as far as possible when dealing with such dispersed data, the proposed average parameters should be a quite good estimation of their "real" value in the highest number of cases.

The values of the hysteretic parameters proposed for modeling are reported in Table 3. Consistently with the calibration procedure adopted, it is recommended to set the type of dissipation to "energy", with $gE = 1$ if the unit of measure of the model are Newtons for forces and millimeters for lengths.

It should be noted that, as already mentioned, the degradation of unloading stiffness due to cyclic loading is modelled by means of a factor equal to $(1-\delta k_i)$ ranging from 1 to $(1-gKLim) = 0.01$ and multiplying the initial stiffness of the response envelope, which has been set to the secant-to-yielding stiffness. For this reason, if the alternative initial stiffness (i.e., the secant-to-40% of yielding moment one) is adopted for modeling, different values of $gK1$, $gK2$, $gK3$, and $gK4$ should be adopted. The application of the above-described procedures for the re-calibration of gKi parameters provided the following results: $gK1 = 0.071$; $gK2 = 0.048$; $gK3 = 0.628$; $gK4 = 0.106$. These values are notably similar to those already presented but provide at given d_i and E_i values, higher values of δk_i. This is expected, since the application of Eq. 11 with K_0 equal to K_{40} and with the second set of gKi values should provide the same result of the same formulation applied with K_0 equal to K_y and with the set of gKi values provided in Table 3. Since K_{40} is higher than K_y, higher values of δk_i are needed to achieve this goal.

6 Application of the proposed model

The proposed equations for the assessment of the response envelope are applied on the subsets of the selected database from which they have been derived. For comparison, on the same subsets, also the corresponding equations proposed by Haselton et al. (2008) are applied.

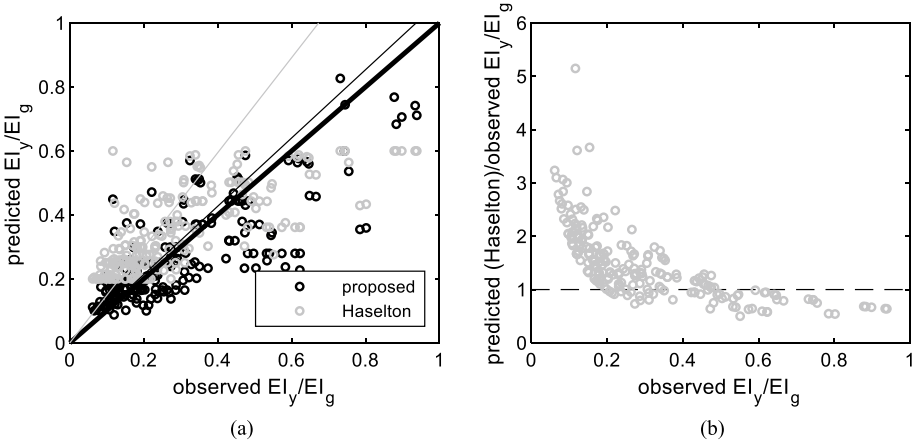

Fig. 9 Assessment of the secant-to-yielding stiffness: comparison between the proposed model outcomes and those produced by Haselton's model (**a**); systematic overestimation of the secant-to-yielding stiffness by Haselton model for specimens with very low secant-to-yielding stiffness (**b**)

Regarding the secant-to-yielding stiffness, with reference to the considered subset, it is observed in Fig. 9a that, on average, Haselton et al.'s proposal overestimates the secant-to-yielding stiffness. This occurs because the formulation proposed by Haselton sets a lower bound of the secant-to-yielding stiffness equal to 20% of the elastic gross one. In fact, it is observed from Fig. 9b that the maximum overestimation when applying Haselton formulation is registered when dealing with specimens with very low observed secant-to-yielding stiffness, which are included in the considered database. In addition, the dataset considered by Haselton includes specimens with axial load ratio ranging from 0 to 0.80 and slenderness ranging from 2 to 6; the database considered for this study and namely for the derivation of a formulation of the secant-to-yielding stiffness includes tests with axial load ratio ranging from 0 to 0.90 and, above all, slenderness ratio ranging from 1.27 to 8.90. It is observed that specimens with low slenderness (and very low axial load) tend to have very low secant-to-yielding stiffness, even lower than 10% of the elastic gross one.

Regarding the chord rotation at capping/peak load, the comparison between the outcomes of the proposed model and of Haselton model is shown in Fig. 10. Haselton model overestimates the observed values of the chord rotation at capping/peak load because it does not consider the effect cyclic degradation when predicting the response envelope.

Similar considerations can be extended for the values of the chord rotation at conventional ultimate and at collapse, as shown in Fig. 11a. Note that Haselton model does not provide a direct formulation for the calculation of the chord rotation at conventional ultimate (i.e., at 20% strength degradation with respect to peak moment). So, it has been calculated by summing the predicted chord rotation at capping plus the 20% of the predicted post-capping chord-rotation capacity. In addition, the outcomes of the proposed model are compared also with the outcomes of the formulation of the chord rotation at conventional ultimate of ductile rectangular RC columns proposed by Biskinis and Fardis (2010) and also by Eurocode 8 (2004) in Fig. 11b. Note that the results of the formulation by Biskinis and Fardis must be multiplied for a coefficient equal to 0.85 if the column is not provided of seismic detailing: since this information is not given in the considered database (see Sect. 3), the formulation is applied two times (with and without 15% reduction of the result) and, so, for each observed value of the chord rotation at ultimate a couple of

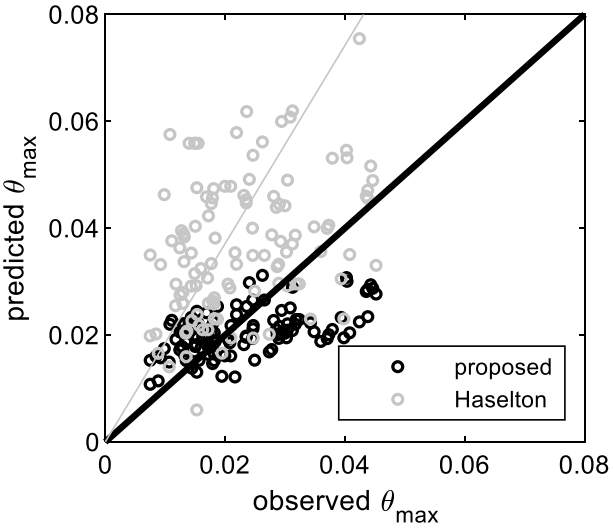

Fig. 10 Assessment of the chord rotation at capping/peak load: comparison between the proposed model outcomes and those produced by Haselton's model

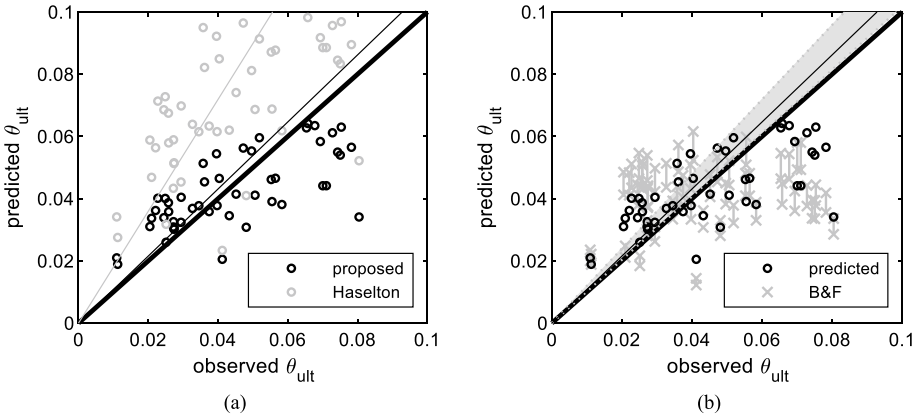

Fig. 11 Assessment of the chord rotation at conventional ultimate: comparison between the proposed model outcomes and those produced by Haselton's model (**a**) and by Biskinis and Fardis's formulation (**b**). Note that the average prediction by Biskinis and Fardis's formulation falls within the grey-shaded area due to the uncertainties related to the presence of seismic detailing in the considered specimens

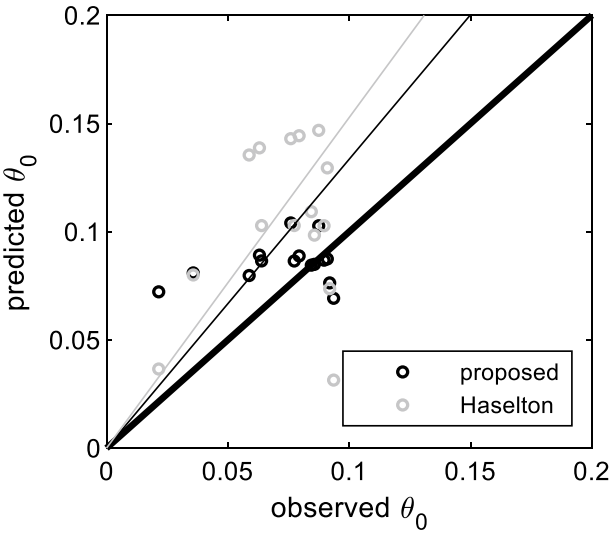

Fig. 12 Assessment of the chord rotation at collapse: comparison between the proposed model outcomes and those produced by Haselton's model

predictions are obtained (a lower bound one and an upper bound one). The formulation by Biskinis and Fardis was derived on a very large database and has been applied by accounting for the effects of cyclic loading. As shown in Fig. 11b, it provides results in very good accordance with the experimental ones, with a limited bias.

Note that the proposed prediction of the chord rotation at collapse (Fig. 12) is affected by a higher bias with respect to the prediction of the other deformation capacity limits, even if still lower than the bias associated with Haselton's formulation (that does not explicitly account for cyclic degradation). This occurs because of the high dispersion of data and, above all, because the proposed model defines each deformation capacity limit

Table 4 Statistics of the observed-to-predicted ratios calculated for both the proposed model and Haselton model outcomes

Response parameter	Observed-to-predicted ratios with proposed model			Observed-to-predicted ratios with Haselton model		
	Mean	Median	CoV	Mean	Median	CoV
Secant-to-yielding stiffness	1.09	1.00	0.42	0.80	0.76	0.43
Chord rotation at capping	1.11	1.05	0.36	0.67	0.64	0.51
Chord rotation at conventional ultimate	1.04	0.91	0.36	0.64	0.60	0.44
Chord rotation at collapse	0.86	0.89	0.31	0.83	0.62	0.76

(peak load, ultimate and collapse) as the sum of partial plastic rotation contributions. This make the prediction of the collapse rotation the most biased one since it is affected by the sum of the bias of the prediction of each contribution.

Table 4 shows the statistics of the observed-to-predicted ratios calculated by adopting the proposed model and Haselton equations. Note that the statistics reported in Table 4 for the proposed model are different from those presented in Sect. 5.1, since in Sect. 5.1 they are calculated for observed-to-predicted ratios evaluated for "partial/plastic" chord rotation contributions, while in Table 4 they are calculated for "total" chord rotation values. Table 4 entries quantify the general comments already discussed: the proposed and Haselton model are characterized by similar scatter, while the bias is lower for the proposed model, since the equations proposed by Haselton underestimate the observed values of chord rotation at capping, ultimate, and collapse for cyclically tested columns.

Among the hundreds of tests included in the selected database, six tests have been selected in order to show the performance of the proposed hysteretic model: three tests are selected to show, based on the Authors' judgment, the best performances of the proposed model, while three tests are selected to show its worst performances and its potential limits.

The "best" performance of the proposed model has been observed for the reproduction of the cyclic response of specimen No.1 by Soesianawati (1986) of specimen 214-08 by Zhou et al. (1987), and of specimen B2 by Sakai et al. (1990). The experimental vs predicted moment-chord rotation responses for these tests are shown in Fig. 13.

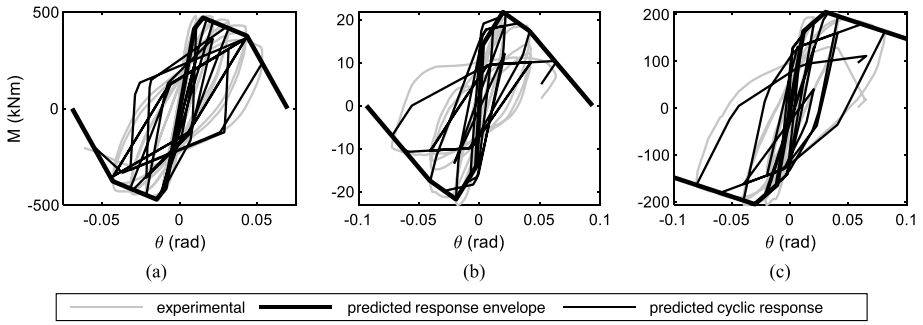

Fig. 13 "Best" predictions of the proposed model: **a** specimen No. 1 by Soesianawati (1986); **b** specimen 214-08 by Zhou et al. (1987); **c** specimen B2 by Sakai et al. (1990)

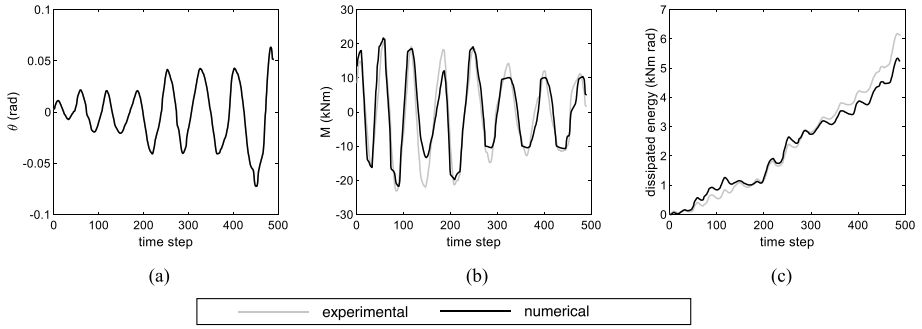

Fig. 14 Predictions of the proposed model for specimen 214-08 by Zhou et al. (1987): **a** experimentally and numerically imposed chord rotations; **b** observed and predicted moment; **c** observed and predicted energy dissipation

For a better comprehension of the proposed model capability in reproducing the cyclic response of an RC column, Fig. 14 shows the evolution with time steps of the observed and predicted imposed displacement (of course, in this case, observed and identical imposed values are shown), moment, and energy dissipation, for test 214-08 by Zhou et al. (1987).

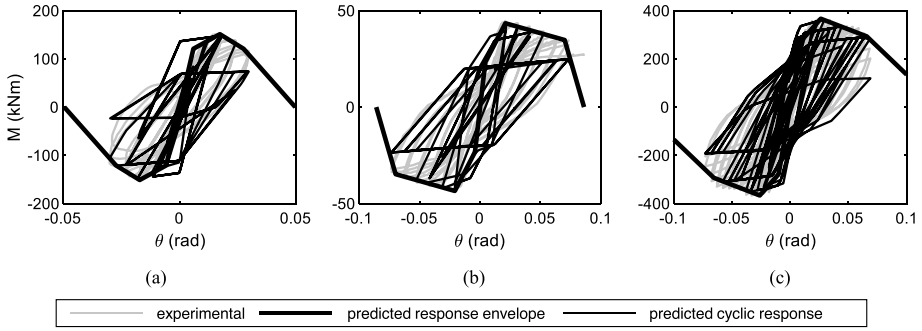

Fig. 15 "Worst" predictions of the proposed model: **a** specimen No. 10 by Atalay and Penzein (1975); **b** specimen C10-05N by Matamoros (1999); **c** specimen C1-1 by Mo and Wang (2000)

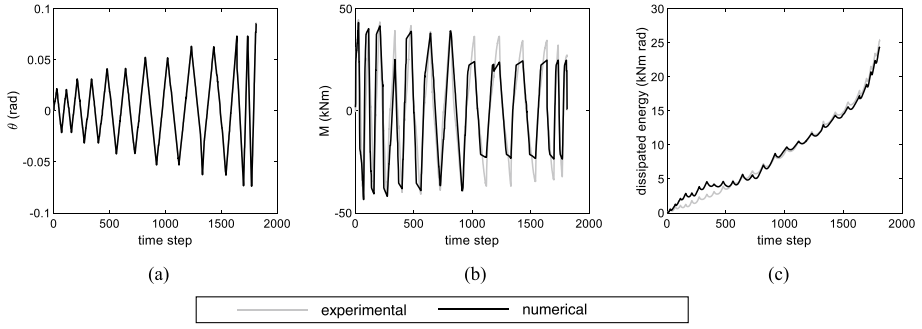

Fig. 16 Predictions of the proposed model for specimen C10-04N by Matamoros (1999): **a** experimentally and numerically imposed chord rotations; **b** observed and predicted moment; **c** observed and predicted energy dissipation

The "worst" performance of the proposed model has been observed for the reproduction of the cyclic response of specimen No. 10 by Atalay and Penzein (1975), of specimen C10-05N by Matamoros (1999), and of specimen C1-1 by Mo and Wang (2000). The experimental versus predicted moment-chord rotation responses for these tests are shown in Figs. 15 and 16.

Note that in the above Figures, the predicted maximum moment is always assumed equal to the observed maximum moment. This has been done in order to propose comparisons between experimental and numerical cyclic responses not biased by the difficulty in the prediction of M_{max}, which, in the case of the proposed model, is determined by applying a flat amplifying factor to M_y, which, in tune, is determined by means of a theoretical fibre section analysis.

It is observed that the proposed model may sometimes fail by predicting an accelerated degradation of reloading stiffness inducing an underestimation of moment capacity, as shown in Fig. 16. However, it should be noted that: (i) of course, the parameters proposed for modeling are "average" values, so it is unavoidable that they will fail the optimal reproduction of specific tests; (ii) the response envelope is well predicted also in the worst cases, thus assuring a quite good prediction of the chord rotation at collapse, despite the overestimation of reloading stiffness degradation that sometimes is observed.

7 Conclusions

In this work, the results of the cyclic experimental on rectangular RC columns with deformed bars included in ACI 369 Rectangular Columns Database have been processed in order to identify significant points of the moment–chord rotation response envelope of these structural members. For ductile columns, four points have been defined: yielding, maximum, conventional ultimate (at 20% strength degradation with respect to maximum moment), collapse (at zero moment capacity). The moment corresponding to these points can be determined by means of mechanical approaches; empirical equations have been derived for the assessment of the chord rotation corresponding to these points. The proposed response envelope already accounts for cyclic strength degradation, since it is calibrated on the response envelope of columns tested under cyclic loads (i.e., monotonic tests are not considered). The proposed response envelope is implemented in OpenSees by adopting the Pinching4 Material model, which also allows considering further sources of cyclic degradation, such as unloading and reloading stiffness degradation, and pinching effect. So, average values of the hysteretic parameters allowing modeling these phenomena are proposed, based on the experimental results included in the selected database. The proposed model is empirical and can be rigorously applied only for columns with geometric and mechanical properties within the ranges defined by the columns of the considered experimental database; in addition, it applied only for ductile columns. So, a simple procedure is proposed to assess if a RC column is ductile and the proposed model is applicable, based on the column geometric and mechanical properties.

The proposed model is applied at the element level and at the structural level, thus showing the advantages and potential limitations of its use. Above all, it is observed that, with respect to other multilinear response models for RC columns with deformed bars, it allows accounting for cyclic strength degradation effects also within nonlinear static analyses, thus allowing a more accurate prediction of the softening response of RC structures.

The performed calibration of the hysteretic parameters for modeling cyclic degradation effects in terms of unloading and reloading stiffness and pinching is highly useful for performing more accurate nonlinear dynamic analyses.

Note that, despite the fact that the calibrated hysteretic parameters are determined for modeling within OpenSees software framework, the proposed equations for the prediction of the response envelope can be adopted for modeling within whichever software allowing implementing "user-defined" response envelopes for RC members.

Appendix

Statistics and predictive capacity of the cyclic response envelope predictive equations

The equations derived to define the response envelope of ductile rectangular RC columns in Sect. 5.1 are herein proposed again with further information regarding their features and their predictive capacity. Remember that in the proposed equations, forces must be expressed in Newtons and lengths in millimetres.

The ratio between secant-to-yielding and gross section stiffness, EI_y/EI_g can be calculated as reported in Eq. 12 (corresponding to Eq. 5).

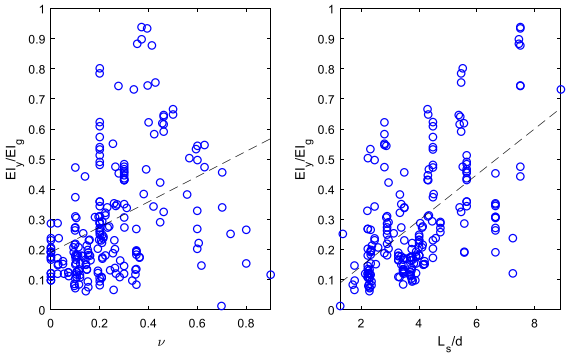

Fig. 17 Trends of the observed secant-to-yielding stiffness with the selected predictors

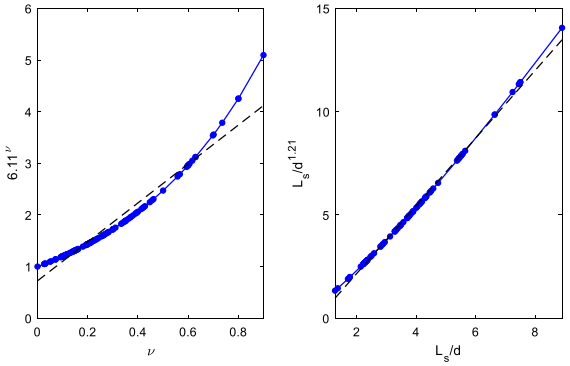

Fig. 18 Trends of the outcomes of the proposed predictive equation for secant-to-yielding stiffness with the variation of the selected predictors

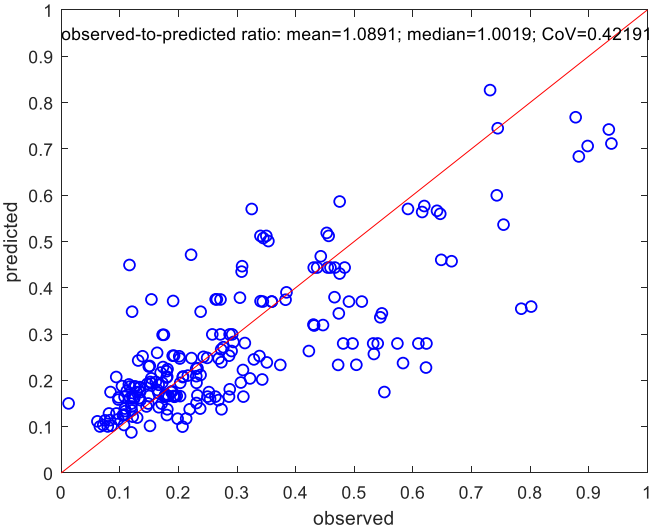

Fig. 19 Comparison between observed and predicted secant-to-yielding stiffness

$$EI_y/EI_g = 0.0318 \cdot 6.11^{\nu} \cdot \left(L_s/d\right)^{1.21} \simeq 0.0318 \cdot 6.11^{\nu} \cdot (1.639\left(L_s/d\right) - 1.110) \quad (12)$$

As shown in Fig. 17, observed values of EI_y/EI_g increase with the axial load ratio and with the column slenderness; the same trend is reproduced by the members of the proposed equation, as shown in Fig. 18. A comparison between the observed and predicted values of EI_y/EI_g is shown in Fig. 19, together with the statistics of the observed-to-predicted ratios.

The post-yielding plastic chord rotation, $\theta_{max}{}^{pl}$ can be calculated as reported in Eq. 13 (corresponding to Eq. 7).

$$\theta_{max}^{pl} = 0.0073 \cdot 0.436^{\nu} \cdot (s/d)^{-0.261} \cdot 1.05^{100\omega_2} \quad (13)$$

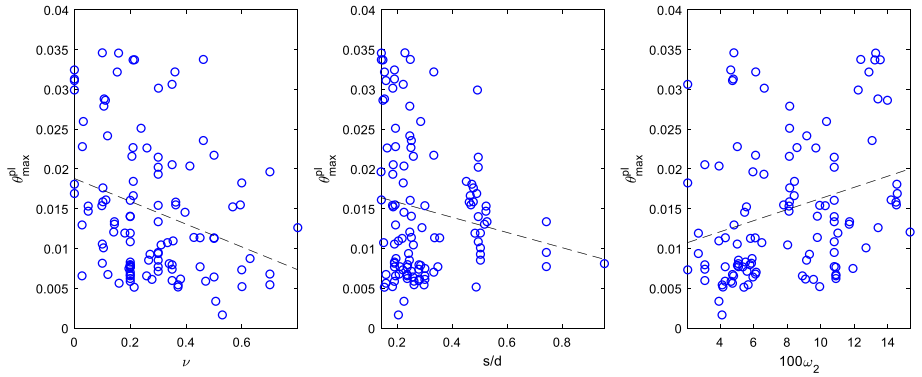

Fig. 20 Trends of the observed post-yielding plastic chord rotation with the selected predictors

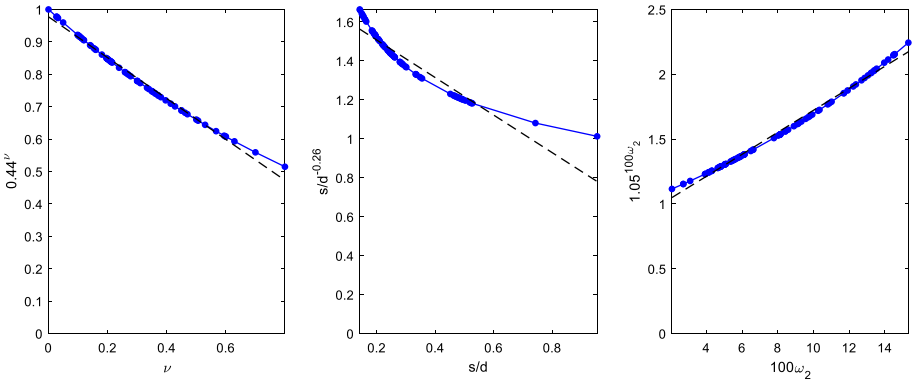

Fig. 21 Trends of the outcomes of the proposed predictive equation for post-yielding plastic chord rotation with the variation of the selected predictors

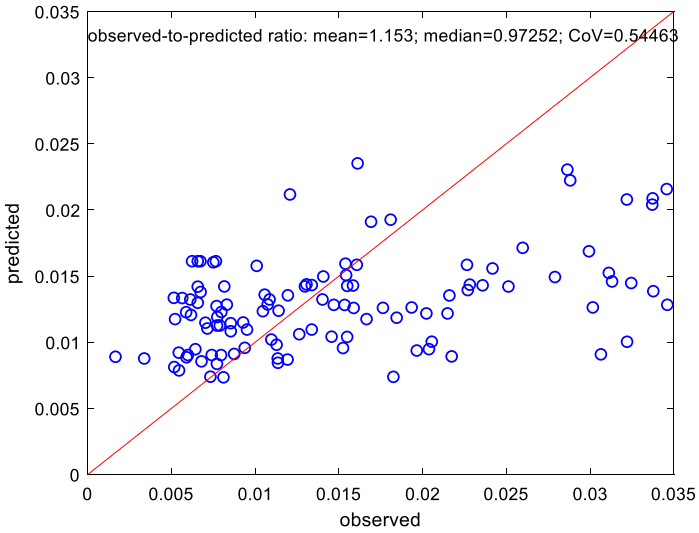

Fig. 22 Comparison between observed and predicted post-yielding plastic chord rotation

As shown in Fig. 20, observed values of $\theta_{max}{}^{pl}$ decrease at increasing the axial load ratio and stirrups spacing-to-effective depth ratio, while they increase at increasing mechanical ratio of longitudinal reinforcement in compression; the same trends are reproduced by the members of the proposed equation, as shown in Fig. 21. A comparison between the observed and predicted values of $\theta_{max}{}^{pl}$ is shown in Fig. 22, together with the statistics of the observed-to-predicted ratios.

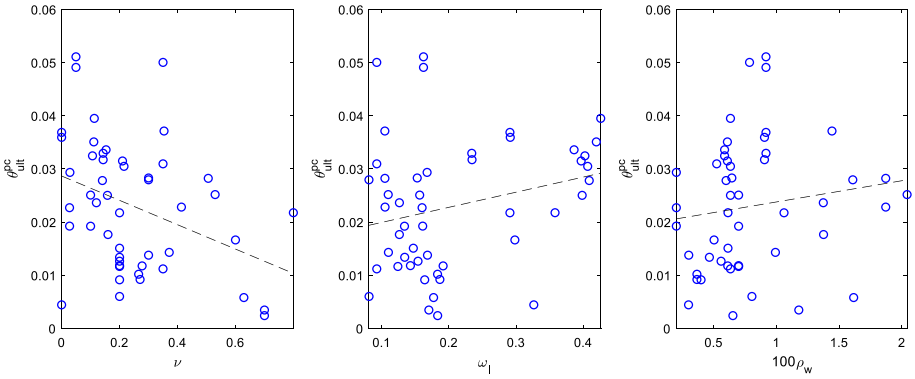

Fig. 23 Trends of the observed post-capping "ultimate" plastic chord rotation with the selected predictors

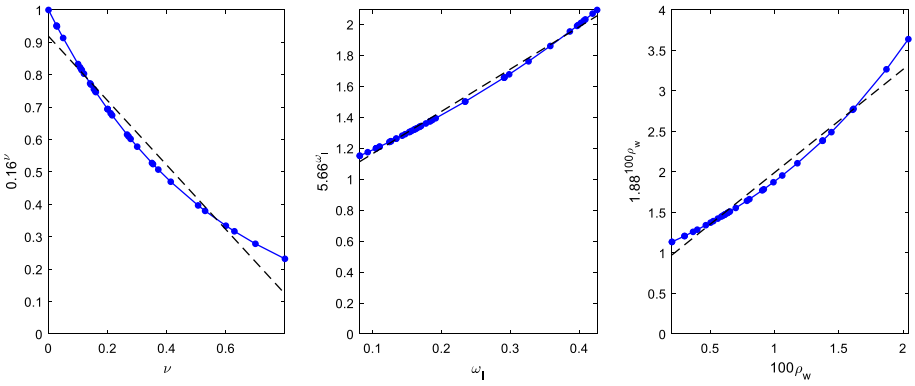

Fig. 24 Trends of the outcomes of the proposed predictive equation for post-capping "ultimate" plastic chord rotation with the variation of the selected predictors

As already mentioned in Sect. 5.1, the calculation of the peak resistance, a simple mean value is proposed attempting to predict the M_{max}/M_y ratio, i.e., $M_{max}/M_y = 1.31$ (observed-to-predicted ratio: CoV = 0.15), with M_y calculated by means of a section fiber analysis.

The post-capping "ultimate" plastic chord rotation, ${\theta_{ult}}^{pc}$ can be calculated as reported in Eq. 14 (corresponding to Eq. 8).

$$\theta_{ult}^{pc} = 0.0126 \cdot 0.161^{\nu} \cdot 5.66^{\omega_l} \cdot 1.88^{100\rho_w} \tag{14}$$

As shown in Fig. 23, observed values of ${\theta_{ult}}^{pc}$ decrease at increasing axial load ratio, while they increase with the mechanical ratio of longitudinal reinforcement and with the geometric ratio of transverse reinforcement; the same trends are reproduced by the members of the proposed equation, as shown in Fig. 24. A comparison between the

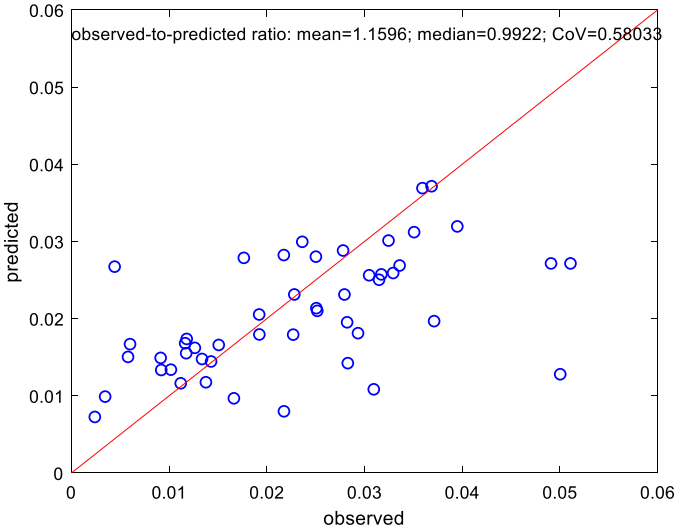

Fig. 25 Comparison between observed and predicted post-capping "ultimate" plastic chord rotation

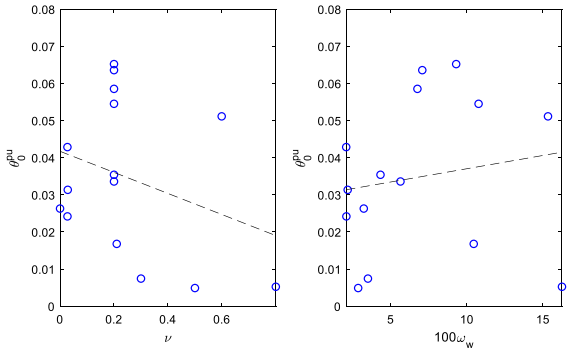

Fig. 26 Trends of the observed post-ultimate plastic chord rotation towards zero resistance with the selected predictors

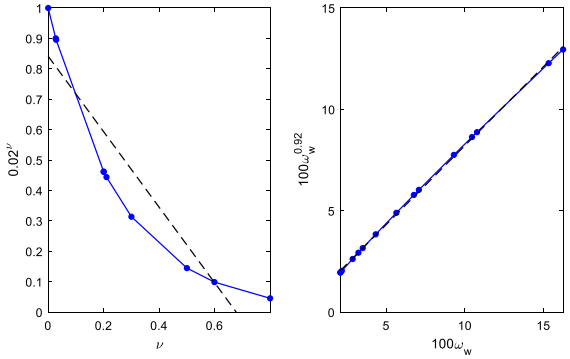

Fig. 27 Trends of the outcomes of the proposed predictive equation for post-ultimate plastic chord rotation towards zero resistance with the variation of the selected predictors

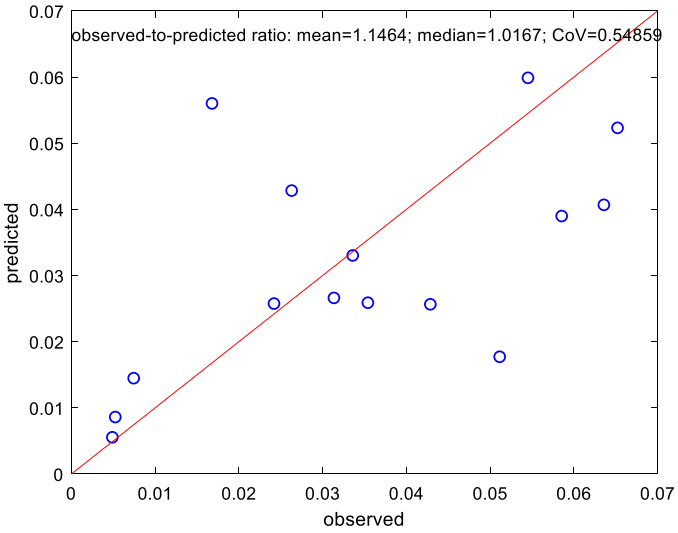

Fig. 28 Comparison between observed and predicted post-ultimate plastic chord rotation towards zero resistance

observed and predicted values of $\theta_{ult}{}^{cl}$ is shown in Fig. 25, together with the statistics of the observed-to-predicted ratios.

The post-ultimate plastic chord rotation towards zero resistance, $\theta_0{}^{pu}$ can be calculated as reported in Eq. 15 (corresponding to Eq. 9).

$$\theta_0^{pu} = min\left(0.065;0.0146 \cdot 0.021^{\nu} \cdot \left(100\omega_w\right)^{0.918}\right) \tag{15}$$

As shown in Fig. 26, observed values of $\theta_0{}^{pu}$ decrease at increasing axial load ratio, while they increase with the mechanical ratio of transverse reinforcement; the same trends are reproduced by the members of the proposed equation, as shown in Fig. 27. A comparison between the observed and predicted values of $\theta_0{}^{pu}$ is shown in Fig. 28, together with the statistics of the observed-to-predicted ratios.

Author contributions All authors contributed to the study conception and design. Material preparation, data collection and analysis were performed by MDD. The first draft of the manuscript was written by MDD and all authors commented on previous versions of the manuscript. All authors read and approved the final manuscript.

Funding This work was developed under the financial support of ReLUIS Research Project – Work Package 11, funded by the Italian Department of Civil Protection, granted to Gerardo M. Verderame.

Data availability The datasets generated during and/or analyzed during the current study are available from the corresponding author on reasonable request.

Declarations

Conflict of interest The Authors have no relevant financial or non-financial interests to disclose.

References

Aboutaha RS, Machado RI (1999) Seismic resistance of steel-tubed high-strength reinforced-concrete columns. J Struct Eng 125(5):485–494

ASCE/SEI American Society of Civil Engineers/Structural Engineering Institute Committee 41 (2017) Seismic evaluation and retrofit of existing buildings (ASCE/SEI 41–17). Reston, Virginia, United States of America

Atalay MB, Penzein J (1975) The seismic behavior of critical regions of reinforced concrete components as influenced by moment, shear and axial force. University of California Berkeley, p 226

Belletti B, Damoni C, Gasperi A (2013) Modeling approaches suitable for pushover analyses of RC structural wall buildings. Eng Struct 57:327–338

Berry M, Parrish M, Eberhard M (2004) PEER structural performance database: user's manual, version 1.0. Pacific earthquake engineering research center. University of California, Berkeley, CA, USA

Biskinis D, Fardis M (2010) Flexure-controlled ultimate deformations of members with continuous or lap-spliced bars. Struct Concr 11(2):93–108

Biskinis DE, Roupakias GK, Fardis MN (2004) Degradation of shear strength of reinforced concrete members with inelastic cyclic displacement. ACI Struct J 101(6):773–783

Bruschi E, Calvi PM, Quaglini V (2021) Concentrated plasticity modelling of RC frames in time-history analyses. Eng Struct 243:112716

Coleman J, Spacone E (2001) Localization issues in force-based frame elements. J Struct Eng 127(11):1257–1265

Di Domenico M, Ricci P, Verderame GM (2021) Empirical calibration of hysteretic parameters for modeling the seismic response of reinforced concrete columns with plain bars. Eng Struct 237:112120

Elwood KJ, Eberhard M (2009) Effective stiffness of reinforced concrete columns. ACI Struct J 106(4):476–484

Ghannoum WM (2017) Re-evaluation of modeling parameters and acceptance criteria for non-ductile and splice-deficient concrete columns. In: 16th World conference on earthquake engineering. January 9–13, Santiago, Chile

Haselton CB, Liel AB, Taylor-Lange S, Deierlein GG (2008) Beam-column element model calibrated for predicting flexural response leading to global collapse of RC frame buildings. In: PEER report no. 2007/03. Pacific earthquake engineering research center, University of California, Berkeley, CA, USA

Lee CS, Park Y, Jeon J-S (2021) Model parameter prediction of lumped plasticity model for nonlinear simulation of circular reinforced concrete columns. Eng Struct 245:112820

Lima C, Angiolilli M, Barbagallo F, Belletti B, Bergami AV, Camata G, Cantagallo C, Di Domenico M, Fiorentino G, Ghersi A, Gregori A, Lavorato D, Luciano R, Marino EM, Martinelli E, Nuti C, Ricci P, Rosati L, Ruggieri S, Sessa S, Spacone E, Terrenzi M, Uva G, Vecchi F, Verderame GM (2020) Nonlinear modeling approaches for existing Reinforced Concrete buildings: the case study of De Gasperi-Battaglia school building in Norcia. Lect Notes Civ Eng 42:82–95

Lowes LN, Mitra N, Altoontash A (2004) A beam-column joint model for simulating the earthquake response of reinforced concrete frames. In: PEER report no. 2003/10. Pacific earthquake engineering research center, University of California, Berkeley, CA, USA

Ma Y, Gong JX (2018) Probability identification of seismic failure modes of reinforced concrete columns based on experimental observations. J Earthq Eng 22(10):1881–1899

Mander JB, Priestley MJN, Park R (1988) Theoretical stress-strain model for confined concrete. J Struct Eng 114(8):1804–1826

Matamoros AB (1999) Study of drift limits for high-strength concrete columns. Department of Civil Engineering. Urbana (Illinois), University of Illinois at Urbana-Champaign. Doctor of Philosophy, p 484

McKenna F, Fenves GL, Scott MH (2004) OpenSees: open system for earthquake engineering simulation. Pacific earthquake engineering research center. University of California, Berkeley, CA, USA

Melek M, Wallace JW (2004) Cylic behavior of columns with short lap splices. ACI Struct J 101(6):802–811

Mo YL, Wang SJ (2000) Seismic behavior of RC columns with various tie configurations. J Struct Eng 126(10):1122–1130

Priestley MJN, Verma R, Xiao Y (1994) Seismic shear strength of reinforced concrete columns. J Struct Eng 120(8):2310–3239

Priestley MJN, Calvi GM, Kowalsky MJ (2007) Displacement-based seismic design of structures. IUSS Press, Pavia

Rodrigues H, Varum H, Arêde A, Costa A (2012) Comparative efficiency analysis of different nonlinear modelling strategies to simulate the biaxial response of RC columns. Earthq Eng Eng Vib 11:553–566

Rosner B (1983) Percentage points for a generalized ESD many-outlier procedure. Technometrics 25(2):165–172

Sakai Y, Hibi J, Otani S, Hiroyuki A (1990) Experimental study on flexural behavior of reinforced concrete columns using high-strength concrete. Trans Jpn Concr Inst 12:323–330
Scott DW (1979) On optimal and data-based histograms. Biometrika 66:605–610
Sezen H, Moehle JP (2004) Shear strength model for lightly reinforced concrete columns. J Struct Eng 130(11):1692–1703
Sivaramakrishnan B (2010) Non-linear modeling parameters for reinforced concrete columns subjected to seismic loads. The University of Texas at Austin. PhD Dissertation
Soesianawati MT (1986) Limited ductility design of reinforced concrete columns. University of Canterbury, Christchurch, p 208
Spacone E, Ciampi V, Filippou FC (1996) Mixed formulation of nonlinear beam finite element. Comput Struct 58(1):71–83
Terrenzi M, Spacone E, Camata G (2020) Comparison between phenomenological and fiber-section nonlinear models. Front Built Environ 6:38
Vafei M, Alih SC, Fallah A (2019) The accuracy of the lumped plasticity model for estimating nonlinear behavior of reinforced concrete frames under gradually increasing vertical loads. Struct Concr 21(1):65–80
Verderame GM, Ricci P (2018) An empirical approach for nonlinear modeling and deformation capacity assessment of RC columns with plain bars. Eng Struct 176:539–554
Watson S (1989) Design of reinforced concrete frames of limited ductility. Department of Civil Engineering. University of Canterbury, Christchurch, New Zealand. Doctor of Philosophy, p 248
Zhou X, Satoh T, Jiang W, Ono A, Shimizu Y (1987) Behavior of reinforced concrete short column under high axial load. Trans Jpn Concr Inst 9:541–548